

## Negative capacitances in low-mobility solids

H. H. P. Gommans, M. Kemerink,\* and R. A. J. Janssen

*Department of Applied Physics, Eindhoven University of Technology, 5600 MB Eindhoven, The Netherlands*

(Received 29 June 2005; revised manuscript received 3 October 2005; published 15 December 2005)

The negative capacitance as often observed at low frequencies in semiconducting devices is explained by bipolar injection in diode configuration. Numerical calculations are performed within the drift-diffusion approximation in the presence of bimolecular recombination of arbitrary strength. Scaling relations for the characteristic frequency with bias, sample dimensions, and carrier mobilities are presented in the limits of weak and strong recombination. Finally, impedance measurements conducted on a light-emitting diode and photovoltaic cell based on low-mobility organic semiconductors are modeled as a function of bias and temperature, respectively.

DOI: [10.1103/PhysRevB.72.235204](https://doi.org/10.1103/PhysRevB.72.235204)

PACS number(s): 72.20.Jv, 73.61.Ph, 05.60.Cd

### I. INTRODUCTION

Admittance spectroscopy has proven to be a powerful and nondestructive method to study transport properties in dielectric materials. Recently, negative capacitances have been reported on a variety of devices that were based on organic materials<sup>1-4</sup> or on crystalline or amorphous inorganic semiconductors.<sup>5-14</sup> Equally numerous explanations for this negative capacitance (NC) have been presented that involved minority carrier flow,<sup>1,3-5</sup> interface states,<sup>9,13</sup> slow transient time of injected carriers,<sup>14</sup> charge trapping,<sup>2,3,10-12</sup> or space charge.<sup>6</sup> The bulk of these descriptions are either based on phenomenological arguments or based on device representation in an equivalent circuit. However, such representations are not necessarily related to the physical properties of the system, despite the fact that they mimic the measured spectra.

Here we will derive the NC from numerical solutions for Boltzmann transport in the drift-diffusion approximation for bipolar transport. Such a description will provide a general understanding that includes the phenomena of minority carriers, space charge, recombination, and the slow transient time of the injected carriers. In order to conduct such a general investigation, interface and trap states are not considered, although their effect on the capacitance is beyond dispute. We will demonstrate the NC behavior in diode configuration for various recombination rates and successively present numerical scaling relations in the limiting cases in terms of recombination strength, sample dimensions, bias, and carrier mobilities.

The second part of this paper mainly serves as an experimental illustration of preceding numerical section. Here, the negative capacitance is experimentally determined for two devices based on low-mobility organic semiconductors: a light-emitting diode (LED) and a photovoltaic cell (PVC). For the active layer in the LED the PPV derivative MDMO-PPV is used, which has attracted worldwide attention in academia and industry for its favorable combination of solubility and optoelectronic properties. The PVC consists of a blend of MDMO-PPV and a methanofullerene (PCBM) that has demonstrated a power conversion efficiency of 2.5%.<sup>15,16</sup>

Admittance spectra on MDMO-PPV-based LED's have previously been reported as a function of bias.<sup>1,3</sup> It was ob-

served that the light onset coincided with the onset for the NC,<sup>1</sup> which is a strong indication for the existence of a relation between minority carrier (electron) flow and the occurrence of a negative capacitance. This is indeed found to be the case, and we demonstrate that on basis of characteristic features in the capacitance it is possible to determine the two carrier mobilities and recombination rate simultaneously as a function of bias and temperature.

The advantage over alternative electrical characterization techniques such as  $I$ - $V$  characterization or time-of-flight (TOF) in the determination of the minority carrier mobility is that there is no need for modifications of the original device. In  $I$ - $V$  characterization the majority carrier contribution is generally repressed by altering the contacts. In TOF measurements film thicknesses are restricted to values much larger than the optical absorption depth, which is usually far above the thickness used in typical, performance-optimized devices. Submitting to these requirements unintentionally leads to altering the transport properties of the system.

Moreover, it will be demonstrated that in the case the frequency range is sufficiently large, recombination rate constants can be determined.

### II. THEORY

The set of coupled partial differential equations is given by

$$\begin{aligned}\bar{\nabla} \cdot (\epsilon \bar{\nabla} \phi) &= q(n - p), \\ \bar{\nabla} \cdot \bar{\mathbf{J}}_n &= -q(-\partial_t n - R), \\ \bar{\nabla} \cdot \bar{\mathbf{J}}_p &= q(-\partial_t p - R), \\ \bar{\mathbf{J}}_n &= q(D_n \bar{\nabla} n - \mu_n n \bar{\nabla} \phi), \\ \bar{\mathbf{J}}_p &= q(-D_p \bar{\nabla} p - \mu_p p \bar{\nabla} \phi),\end{aligned}\tag{1}$$

where  $\phi$  denotes the electric potential,  $n$  and  $p$  are the free carrier concentrations of electrons and holes, and  $J_n$  and  $J_p$  are the electron and hole current density, respectively.  $D_n$ ,

$D_p$ ,  $\mu_n$  and  $\mu_p$  are the diffusion coefficients and the mobilities of electrons and holes, respectively.  $R$  is the recombination rate and  $\varepsilon = \varepsilon_r \varepsilon_0$  with  $\varepsilon_0$  the permittivity of vacuum and  $\varepsilon_r$  the relative permittivity that is assumed constant. The Einstein relation for diffusion,  $D_{n/p} = k_B T / q \mu_{n/p}$ , is assumed to hold, where  $k_B$  is the Boltzmann constant,  $T$  the temperature, and  $q$  the elementary charge.

Numerical solution of the above system of equations is far from trivial. The system of equations is singularly perturbed<sup>17</sup> and highly nonlinear. Dedicated numerical methods have been developed to solve the system, and they turn out to be essential for a robust and efficient solution. The Scharfetter-Gummel discretization scheme must be used to discretize the current densities, whereas damped Newton methods<sup>18</sup> or nonlinear variable transformations<sup>19</sup> are essential for the solution of the extremely nonlinear systems of discretized equations. A thorough description of all numerical methods used for semiconductor device simulation will be given in Ref. 20. The simulations described in this paper have been performed using the software package CURRY, developed within the Philips electronics company. As only a small harmonic modulation is generally applied in admittance spectroscopy, the solutions are linearized in time.

In the case diffusion currents are neglected, a zero electric field is the logical boundary condition at an Ohmic contact. When including diffusion, it is more realistic to apply the free carrier density at the interface,  $\rho_i$ , for the boundary condition, according to

$$\rho_i = n_{\text{metal}} \exp\left(-\frac{\Delta\phi}{kT}\right),$$

with  $\Delta\phi$  the effective barrier height for carrier injection from the metal Fermi level into the transport level of the dielectric and  $n_{\text{metal}}$  the carrier density in the metal. As an Ohmic contact is required to probe the bulk properties,  $\Delta\phi$  must be small ( $\leq 0.2$  eV) and  $\rho_i$  may become unrealistically large—i.e., larger than the density of states (DOS) of the dielectric. Hence, in order to model an Ohmic contact, we set  $\rho_i$  equal to the DOS of the dielectric ( $= 10^{21} \text{ cm}^{-3}$ ). As the number of intrinsic charges in the polymer material under investigation is negligible, space-charge effects become important. In the description of the polymer LED a non-Ohmic contact will be considered for electron injection and hence a smaller charge concentration will be used at the metal-polymer interface. Up to the experimental section the NC will be studied solely from these transport equations.

In the absence of gap states the recombination is given by the bimolecular recombination rate  $R = \gamma np$ , where  $\gamma$  is the recombination rate constant.<sup>21</sup> This constant is generally set equal to  $\gamma_L = e(\mu_n + \mu_p) / (\varepsilon_0 \varepsilon_r)$  as derived by Langevin,<sup>22</sup> although smaller values have been generally found in disordered molecular<sup>23</sup> and inorganic materials.<sup>24</sup> For this reason the capacitance is calculated for a variety of recombination rate constants in diode configuration assuming bipolar injection from Ohmic contacts; see Fig. 1. The material parameters as used in the calculations are given in the figure caption.

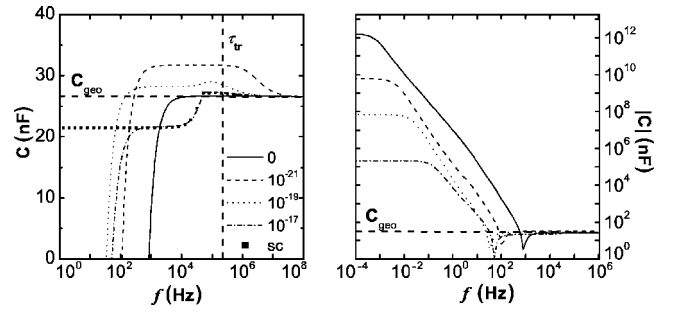


FIG. 1. Left: calculated capacitance  $C(f)$  in a dielectric medium for various recombination constants  $\gamma$  (as given in the inset in  $\text{cm}^3/\text{s}$ ). Here the layer thickness  $L$  is 100 nm, the surface area  $A$  is  $1 \text{ cm}^2$ , the relative permittivity  $\varepsilon_r$  is 3, the bias is 5 V, and the mobility for holes,  $\mu_p$ , is  $10^{-6} \text{ cm}^2/(\text{V s})$  and electrons,  $\mu_n$ , is  $10^{-12} \text{ cm}^2/(\text{V s})$ . The geometrical capacitance is indicated with  $C_{\text{geo}}$  and the single carrier (hole only) with sc. Right: absolute value of the capacitance,  $|C(f)|$ . The used parameters give a Langevin recombination constant  $\gamma_L = 6 \times 10^{-13} \text{ cm}^3/\text{s}$ .

First note that the negative capacitance for bipolar injection is indeed found in the drift-diffusion approximation. At sufficiently low frequencies all capacitances converge to a constant negative value, while at sufficiently high frequencies the geometrical capacitance is obtained. The physical argument for the NC is equivalent to the well-known reduction of the capacitance to  $\frac{3}{4}$  of the geometrical capacitance  $C_{\text{geo}}$  for unipolar space-charge-limited currents at frequencies below the reciprocal transit time.<sup>25</sup> Since the (differential) capacitance reflects the (change in) stored charge per (change in) bias, the presence of (additional) space charge in the dielectric gives rise to a deviation  $\Delta C$  from the geometrical capacitance. Since the buildup of space charge necessarily lags behind the stimulus,  $\Delta C$  is negative. For bipolar currents, the amount of stored space charge can, depending on the recombination strength, be much larger than in the unipolar situation due to the compensation of positive- and negative-charge carriers.<sup>26</sup> Hence the magnitude of  $\Delta C$  is enhanced as well and the total capacitance  $C_{\text{geo}} + \Delta C$  may become negative. The relevant time scales can be best understood in the carrier transient response to a step potential:<sup>14</sup> For a short time period after the voltage step, such that even the fastest carriers cannot respond, only the displacement current contributes to the (geometrical) capacitance, which is determined by the dielectric permittivity. Subsequently, as both injection contacts are set Ohmic, the fastest carriers (holes) will determine the transient field in the following time interval. This field is maintained until the second (electron) carrier response sets in, resulting in modification of this (hole dominated) transient field. However, this modification is closely followed by the hole response. For each time unit the hole and electron current will increase until the field and, thus, the currents have converged towards their final equilibrium configuration, which therefore is determined by both mobilities and the recombination rate. At high recombination rates space charge will dominate the electric field in the whole dielectric layer. For smaller recombination rates the area that is dominated by space charge will decline up to near the injecting contacts. Finally, for zero recombination

this area is confined to the immediate vicinity of the contacts while in the remaining of the layer the field is simply  $V/L$ , where  $V$  is the applied bias and  $L$  is the distance between the electrodes.

From Fig. 1 it can be immediately observed that indeed the recombination rate highly affects the capacitance. At a high recombination rate ( $\gamma=10^{-17}$  cm<sup>3</sup>/s) the frequency-resolved capacitance clearly exhibits a transition from 21.5 to 26.6 nF at  $\sim 10$  kHz that is absent for lower recombination rates. This transition is a consequence of the (positive) space charge and corresponds to the transit time effect as obtained for a single-carrier space-charge-limited configuration that was discussed above. Shao and Wright<sup>25</sup> demonstrated this effect for drift-only transport and calculated that the capacitance at frequencies smaller than the transit time,  $\tau_{tr}=(2L)^2(3\mu_p V)^{-1}$ , is exactly  $\frac{3}{4}$  of the geometrical capacitance. Although this “low”-frequency capacitance slightly differs in the case diffusion is accounted for, the characteristic reciprocal transit time in the frequency domain is exactly reproduced as indicated by the vertical dashed line in Fig. 1.

With decreasing recombination the low-frequency saturation value of the (negative) capacitance increases in magnitude, as expected from the discussion above. In the limit of zero recombination, space-charge effects become negligible and the contacts determine the ac response. Here it is observed that the transition from the constant negative capacitance towards the (constant) geometrical capacitance covers exactly six decades in the frequency domain, corresponding to the six-order-of-magnitude difference in carrier mobility. In fact, this transition is observed to decrease in the frequency range with increasing recombination rate. This can be understood in relation to the foregoing discussion in the transient response picture: The equilibrium electron concentration throughout the dielectric layer is much smaller for the space-charge-dominated field than in case of zero recombination, and hence fewer electrons have to penetrate the layer not as far in order to reach equilibrium.

In the admittance experiments on polymer-based devices the NC will be examined to determine the minority carrier mobility and where possible the recombination constant. In this analysis we will use the frequency  $f_0$  for which  $C(f_0)=0$  as characteristic for the (reciprocal) time scale on which the bimolecular current reaches equilibrium. In Fig. 2, the calculated  $f_0$  is shown for variations in the electron and hole mobilities, the applied bias, and the layer thickness that appear meaningful in experimental configurations. It is shown that for all combinations within this range  $f_0$  can be scaled onto a straight curve by  $f_0 \propto (V/L^2)(\mu_n \mu_p)^{0.62}$ . Variations in  $\mu_p$  are explicitly indicated in Fig. 2. The power in the mobilities is a numerical approximation that, considering the experimental limitations, yields sufficient accuracy. The recombination constant as chosen here ( $0.01 \gamma_L$ ) leads to a space-charge-dominated field and can thus be considered a strong recombination; taking a larger recombination constant consequently leads to the same scaling. The variations in height for the different hole mobilities in Fig. 2 are due to their effect on the recombination rate constant  $\gamma_L$ .

Although it is dangerous to use hand waving arguments to interpret such complex phenomena as bipolar impedance

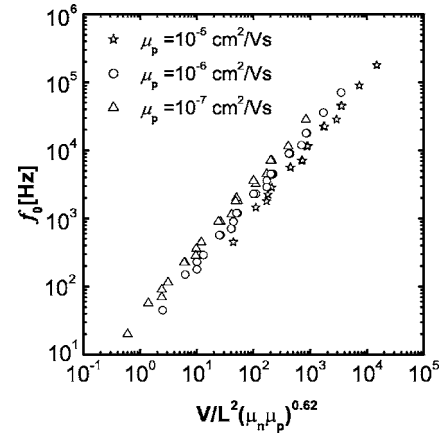


FIG. 2. Calculated zero capacitance frequency  $f_0$  for different bias (2–10 V), layer thickness (50–200 nm), electron mobility [ $10^{-9}$ – $10^{-7}$  cm<sup>2</sup>/(V s)], and hole mobility [ $10^{-7}$ – $10^{-5}$  cm<sup>2</sup>/(V s)]. The recombination constant was chosen to be  $0.01 \gamma_L$ . The remaining parameters were set as in Fig. 1.

spectra, we believe one can qualitatively understand the scaling behavior of  $f_0$ . We start from the well-known Parmenter-Ruppel expression for the bipolar space-charge-limited current in steady state:

$$J \propto \epsilon_0 \epsilon_r \sqrt{\frac{\mu_e \mu_h (\mu_e + \mu_h)}{\mu_r}} \frac{V^2}{L^3},$$

where  $\mu_r$  is the recombination mobility that for Langevin-type recombination is given by  $\mu_r \propto \mu_n + \mu_p$ . Therefore, we have  $J \propto \epsilon_0 \epsilon_r \sqrt{\mu_e \mu_h} V^2 / L^3$ . Now, by analogy with the unipolar situation, where the characteristic frequency of a space-charge-limited current of magnitude  $J \propto \epsilon_0 \epsilon_r \mu V^2 / L^3$  is given by  $f \propto \mu V / L^2$ , one expects for  $f_0$  that  $f_0 \propto \sqrt{\mu_e \mu_h} V / L^2$ . Surprisingly, the scaling that follows from the exact model differs from this prediction only in the exponent of the mobility, despite the fact that both diffusion and the large carrier densities near the contacts are ignored.

In the case the recombination rate is set zero we obtain similar results as in Fig. 2 by scaling  $f_0 \propto \sqrt{\mu_n \mu_p} / L$ . As the bias is always a straightforward tunable variable, this gives a handle to discriminate between the two limits. Obviously, this becomes less straightforward in case the mobility is a function of the electric field<sup>27</sup> or the density.<sup>28</sup>

The temperature dependence of  $C(f)$  in the range of 100–300 K has been calculated in both recombination limits as well, and the results are shown in Fig. 3. It can be observed that for devices with a space-charge-dominated field the temperature and hence the diffusion coefficient  $D$  do not affect the capacitance. This turns out to be very useful as the experimentally derived capacitance can now be directly related to the temperature dependence of the mobilities as will be demonstrated below. This is in contrast to the situation for zero recombination as can be seen in Fig. 3. In our diode configuration the temperature only determines the carrier flow and hence the field near the injecting contacts. In the frequency range where the fastest carriers contribute to the capacitance, the temperature-induced field modifications

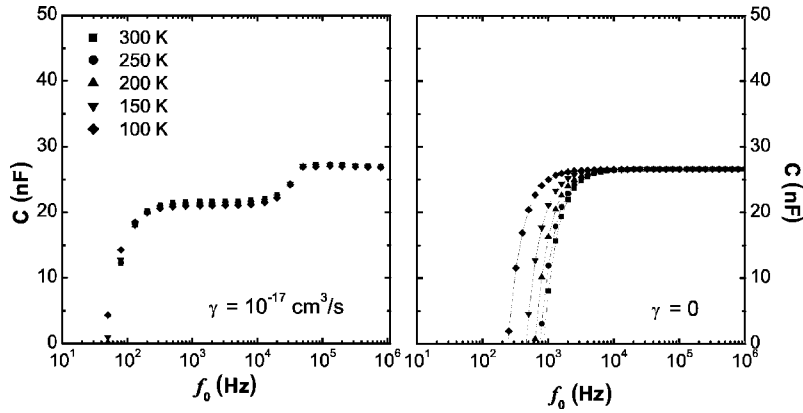


FIG. 3. Calculated capacitance  $C(f)$  in a dielectric medium for  $\gamma=10^{-17}$  cm<sup>3</sup>/s (left) and 0 (right) at different temperatures (see inset). The remaining parameters were set as in Fig. 1.

near the contacts are marginal compared to the space charge in the bulk of the layer in the case of a high recombination rate. However, in case of a low recombination rate, the space charge becomes confined to the direct vicinity of the injecting contacts and hence the capacitance becomes sensitive to temperature changes.

### III. EXPERIMENT

In order to determine the minority carrier mobility in organic devices without modifying the charge injecting contacts, admittance spectroscopy has been conducted on a polymer LED (PLED) and solar cell. Admittance spectroscopy in the range of from 5 Hz to 1 MHz was performed with a Hewlett Packard 4192A impedance analyzer. A small alternating signal  $\nu_{ac}$  of 50 mV was superimposed onto a dc bias  $\nu_{dc}$  up to 7 V.

#### A. PLED

The polymer LED consists of a photoactive layer, poly[2-methoxy-5-(3',7'-dimethyloctyloxy)-1,4-phenylene vinylene] (MDMO-PPV), sandwiched between an indium-tin-oxide (ITO) substrate and Al top layer. In a glovebox filled with a nitrogen atmosphere poly[2-methoxy-5-(3',7'-dimethyloctyloxy)-1,4-phenylene vinylene] MDMO-PPV films were prepared by spin coating a 0.7 wt % toluene solution onto an ITO-coated glass substrate. The film thickness is typically 170 nm as measured by an alpha stepper. By means of a load lock, samples were transported to a UHV chamber for Al deposition without being exposed to air. The LED structures were completed by vapor deposition of an 80-nm Al capping layer. The active area for each LED structure amounts 24 mm<sup>2</sup>. Admittance spectroscopy was conducted *in situ* in the glovebox at a temperature of 20 °C for different forward bias [Fig. 4(b)]. From electroluminescence the onset of light emission was observed at a bias of 4 V. Simultaneously, the negative contribution to the capacitance sets in and is found to extend up to higher frequencies with increasing bias. At 0 V the capacitance equals the geometrical capacitance with a small deviation at higher frequencies (>10 kHz) due to the contact resistance [Fig. 4(a)].

The hole mobility is  $2 \times 10^{-6}$  cm<sup>2</sup>/(V s) at 4–5 V and  $5 \times 10^{-6}$  cm<sup>2</sup>/(V s) at 7 V as determined in our earlier work by the transit time effect.<sup>1</sup> Identical values were determined

from the steady-state conductivity (not shown). The relative permittivity of MDMO-PPV is  $\sim 3$ . Electron injection from the Al into the lowest unoccupied molecular orbital (LUMO) is considered non-Ohmic.<sup>1</sup> Consequently, the charge concentration at the Al interface is included as a constant and determined from the capacitance spectra ( $9 \times 10^{15}$  cm<sup>-3</sup>), just as the recombination rate ( $\gamma_L/1000$ ). Only the electron mobility  $\mu_n$  was optimized for *each* spectrum and the values are given in Fig. 4.

In the determination of these parameters the focus is on the position of the majority carrier transit time effect and the onset of negative capacitance—i.e.,  $f_0$ . In Fig. 4(a) these are observed at  $5 \times 10^4$  and  $2 \times 10^1$  Hz, respectively, and well reproduced by the simulation. The deviation of about 0.5 nF in the range 0.1–10 kHz is fully attributed to the presence of traps,<sup>1</sup> as it has been calculated that trap levels lead to positive contribution to the capacitance.<sup>31</sup> Since their density and distribution in space and energy are unknown,<sup>1</sup> we refrain from taking trap levels into account in our calculations. We believe that this does not significantly affect the values of  $\mu_n$  or  $\gamma$ , for the NC contribution causes a much larger drop in capacitance (from +2.5 to –10 nF) with decreasing frequency than the increase of about 2 nF caused by trap levels.<sup>1,4</sup>

In order to improve the correspondence between the electrical characterization and model descriptions, a distribution in mobility is often applied.<sup>29,30</sup> Here we did not include such

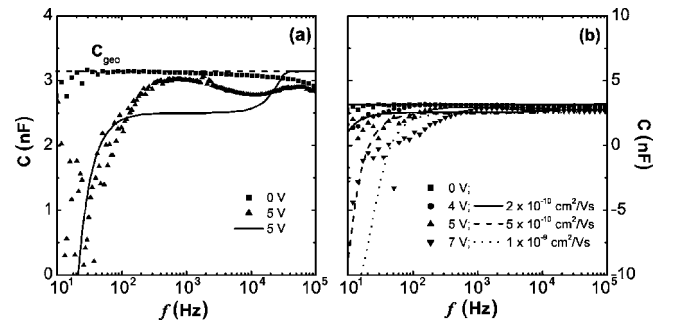


FIG. 4. Measured capacitance  $C(f)$  in a polymer LED structure at 5 V bias (a) and at 4, 5, and 7 V bias (b). The geometrical capacitance is indicated with  $C_{geo}$ . Points are experimental data; lines are calculations using the model outlined in the text. The electron mobilities that are used in the calculations are shown in the inset.

a distribution as the justification for a specific distribution function is not clear<sup>1</sup> and the parameters are unknown *a priori*, but have to be derived from the experimental data. It is beyond the scope of this paper to establish a full description for charge transport in polymer materials as the field and concentration dependence in mobility<sup>27,28</sup> have not been included either. Nevertheless, it should be pointed out that such distributions lead to a smearing out of the transitions in the derivative of the capacitance and hence to an increased correspondence with the experimental data.

As mentioned above, the recombination in organic semiconductors is often calculated according to Langevin.<sup>22</sup> However, in the case the electron mobility is much smaller than the hole mobility this can lead to an unphysically large gradient in the electron concentration (and hence to an unrealistic diffusion current) very near the electron-injecting contact. Consequently, in order to solve the Boltzmann equations a lower recombination rate must be used. Now, as the electron and hole mobility are established by the two characteristic points discussed above, this determines the maximum recombination rate constant to be  $\sim 2 \times 10^{-3} \times \gamma_L$  for the MDMO-PPV layer used in the experiment.

The electron concentration at the Al contact, the recombination rate constant  $\gamma$ , and  $\mu_n$  together determine the slope and the minimum capacitance at frequencies  $< 100$  Hz. Considering the limited agreement with experiment that can be obtained with the present model—i.e., with a constant mobility and without traps—the electron mobility cannot be pinpointed within a factor of 3 or so. This factor is, however, comparable with the experimental sample-to-sample reproducibility. For similar reasons, the uncertainty in the recombination rate constant is about a factor of 5.

Both the electron and hole mobilities exhibit the (apparent) field dependence typically observed in disordered molecular materials,  $\mu_{n/p} = \mu_0 \exp(\beta \sqrt{E})$ . The values of  $\beta$  and  $\mu_0$  that are derived from the extracted values of  $\mu_p$  were found to be in good agreement with values reported in the literature.<sup>1</sup> Since trapping effects, which are of importance in the same frequency range as  $f_0$ , are not accounted for in the model, we refrain from extracting  $\beta$  and  $\mu_0$  from the used values of  $\mu_n$ . Finally, it should be pointed out that the NC cannot directly be related to the electron mobility as was assumed in Ref. 4. According to the method described in Ref. 4, the electron mobility would yield  $4.6 \times 10^{-11}$ ,  $8.4 \times 10^{-11}$ , and  $2.3 \times 10^{-10}$  cm<sup>2</sup>/(V s) for 4, 5, and 7 V bias, respectively, and differs from our result by a factor of  $\sim 20$ .

### B. Bulk heterojunction solar cell

The bulk heterojunction solar cell consists of a blend of donor material MDMO-PPV and electron accepting material 1-(3-methoxycarbonyl)propyl-1-phenyl-[6,6]-fullerene (PCBM). Prior to sample preparation, the ITO-covered glass substrates were cleaned by ultrasonic treatment in acetone, rubbing with soap, rinsing with demineralized water, refluxing with isopropanol, and finally 20-min UV ozone treatment. Subsequently, a 100-nm-thick layer of polyethylenedioxythiophene:polystyrenesulfonate (PEDOT:PSS) was spin coated (1500 rpm, 90 s) from an aqueous disper-

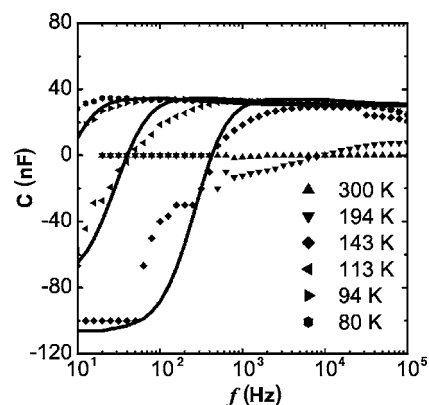


FIG. 5. Measured capacitance  $C(f)$  in an organic solar cell structure at 1.25 V for different temperatures (see inset). Points are experimental data; lines are calculations using the model outlined in the text, using the following (main) parameters. At 143 K,  $\mu_n = 1.3 \times 10^{-6}$  cm<sup>2</sup>/(V s),  $\mu_p = 1 \times 10^{-7}$  cm<sup>2</sup>/(V s), and  $\gamma = 3 \times 10^{-14}$  cm<sup>3</sup>/s =  $0.040 \gamma_L$ . At 113 K,  $\mu_n = 1 \times 10^{-7}$  cm<sup>2</sup>/(V s),  $\mu_p = 2 \times 10^{-8}$  cm<sup>2</sup>/(V s), and  $\gamma = 3 \times 10^{-15}$  cm<sup>3</sup>/s =  $0.047 \gamma_L$ . At 94 K,  $\mu_n = 3 \times 10^{-8}$  cm<sup>2</sup>/(V s),  $\mu_p = 5 \times 10^{-9}$  cm<sup>2</sup>/(V s), and  $\gamma = 1 \times 10^{-15}$  cm<sup>3</sup>/s =  $0.054 \gamma_L$ .

sion under ambient conditions on the cleaned substrates and dried by annealing for 1 min at 180 °C. Then a 90-nm-thick layer was spin coated (1000 rpm, 90 s) on top of the PEDOT:PSS from a chlorobenzene solution consisting of MDMO-PPV and PCBM in the mixing ratio 1:4 by weight, which was stirred vigorously overnight in the dark. The substrates were then transferred into a glovebox filled with nitrogen atmosphere ( $[O_2] < 1$  ppm and  $[H_2O] < 1$  ppm). From there, they were introduced in a vacuum deposition chamber ( $p \sim 10^{-6}$  mbar). Then, 1.0 nm of LiF and 100 nm of Al were deposited right after each other while the sample temperature was kept below 40 °C. Inside the glovebox, the samples were mounted in a variable-temperature continuous-flow cryostat, which was subsequently evacuated. The admittance spectra were taken at various temperatures between 80 and 300 K. At high temperatures ( $> 194$  K) the value of the electron mobility of the PCBM phase is too high to observe significant dielectric behavior. Instead of a capacitance close to the geometrical value, we measure a purely Ohmic resistor and thus zero capacitance. This is due to the specifications of the HP 4192A (the device under test should have a series resistance of  $> 100 \Omega$ ) and thus not due to fundamental reasons. Similar measurements, though on much thicker devices, have been reported in Ref. 33.

The relative permittivity  $\epsilon_r = 3.4$  was determined from the geometrical capacitance. The parameters that are determined from the measured data are the electron and hole mobilities and the recombination constant. Both contacts were assumed Ohmic. The fitting procedure is similar as for the PLED with the important differences that the minimum (negative) value for the capacitance was now clearly resolved at 113–143 K (Fig. 5) and that traps are not relevant in absence of illumination. As a result, the variation in  $\gamma$  that matches the capacitive minimum is, for a fixed set of mobilities, very narrow (within 10%). This is well within the experimental accuracy of the mobility (about a factor of 3), which is determined by

the reproducibility. The model gives thus an accurate description of the data in the entire frequency range. From these simulations, the recombination constant was determined to be  $\gamma = \gamma_L/25$ ,  $\gamma = \gamma_L/21$ , and  $\gamma = \gamma_L/19$  at 143, 113, and 94 K, respectively. These results suggest that the recombination rate constant converges towards the Langevin value with decreasing temperature. Similar results were found before by Nelson who used a temperature-dependent ratio between free and trapped positive polarons to explain this.<sup>32</sup>

The overestimation in the low-frequency slope of the capacitance is found in these blends as well. This again may be attributed to a distribution in mobility and/or the presence of two different charge-transporting phases in the blend.

In summary, we demonstrate that in a metal-insulator-metal configuration the time-dependent drift-diffusion equations result in a negative capacitance for bipolar transport. At high recombination rates, the frequency for zero capacitance,  $f_0$ , is found to scale as  $f_0 \sim (\mu_n \mu_p)^{0.62} V/L^2$ . At zero recombination rate, we find  $f_0 \sim \sqrt{\mu_n \mu_p}/L$ .

Two examples of capacitance spectra on low-mobility-charge transporting layers exhibiting negative capacitances are shown. For the polymer LED, hole and (approximate) electron mobilities were determined as a function of bias. In the case of the bulk heterojunction photovoltaic cell the mobilities together with the recombination rate constant were obtained at different temperatures. Finally, we conclude that the capacitance spectra provide an elegant way to directly determine the minority carrier mobility and recombination rate constant without making modifications to the device.

## ACKNOWLEDGMENTS

This research was supported by grants from the Dutch Foundation for Material Research (FOM). We thank R.M.T. Pijper and J.M. Kramer for the experimental data, M.M. Wienk for supplying the organic materials, and W.H.A. Schilders for making available the CURRY software package.

\*Author to whom correspondence should be addressed. Electronic address: m.kemerink@tue.nl

<sup>1</sup>H. H. P. Gommans, M. Kemerink, G. G. Andersson, and R. M. T. Pijper, *Phys. Rev. B* **69**, 155216 (2004).

<sup>2</sup>L. S. C. Pingree, B. J. Scott, M. T. Russell, and M. C. Hersam, *Appl. Phys. Lett.* **86**, 073509 (2005).

<sup>3</sup>I. N. Hulea, R. F. J. van der Scheer, H. B. Brom, B. M. W. Langeveld-Voss, A. van Dijken, and K. Brunner, *Appl. Phys. Lett.* **83**, 1246 (2003).

<sup>4</sup>H. C. F. Martens, J. N. Huiberts, and P. W. M. Blom, *Appl. Phys. Lett.* **77**, 1852 (2000).

<sup>5</sup>J. Werner, A. F. J. Levi, R. T. Tung, M. Anzlowar, and M. Pinto, *Phys. Rev. Lett.* **60**, 53 (1987).

<sup>6</sup>G. B. Parravicini, A. Stella, M. C. Ungureanu, and R. Kofman, *Appl. Phys. Lett.* **85**, 302 (2004).

<sup>7</sup>V. Kytin, Th. Dittrich, F. Koch, and E. Lebedev, *Appl. Phys. Lett.* **79**, 108 (2001).

<sup>8</sup>J.-C. M'Peko, *Appl. Phys. Lett.* **77**, 735 (2000).

<sup>9</sup>A. G. U. Perera, W. Z. Shen, M. Ershov, H. C. Liu, M. Buchanan, and W. J. Schaff, *Appl. Phys. Lett.* **74**, 3167 (1999).

<sup>10</sup>F. Lemmi and N. M. Johnson, *Appl. Phys. Lett.* **74**, 251 (1999).

<sup>11</sup>N. C. Chen, P. Y. Wang, and J. F. Chen, *Appl. Phys. Lett.* **72**, 1081 (1998).

<sup>12</sup>K. Ždánský, *J. Appl. Phys.* **88**, 2024 (2000).

<sup>13</sup>X. Wu, E. S. Yang, and H. L. Evans, *J. Appl. Phys.* **68**, 2845 (1990).

<sup>14</sup>M. Ershov, H. C. Liu, L. Li, M. Buchanan, Z. R. Wasilewski, and A. K. Jonscher, *IEEE Trans. Electron Devices* **45**, 2196 (1998) and reference therein.

<sup>15</sup>S. E. Shaheen, C. J. Brabec, N. S. Sariciftci, F. Padinger, T. Fromherz, and J. C. Hummelen, *Appl. Phys. Lett.* **78**, 841 (2001).

<sup>16</sup>C. J. Brabec, S. E. Shaheen, C. Winder, N. S. Sariciftci, and P.

Denk, *Appl. Phys. Lett.* **80**, 1288 (2002).

<sup>17</sup>P. A. Markowich, *SIAM J. Appl. Math.* **44**, 896 (1984).

<sup>18</sup>R. E. Bank and D. J. Rose, *Numer. Math.* **37**, 279 (1981).

<sup>19</sup>S. J. Polak, C. den Heijer, W. H. A. Schilders, and P. A. Markowich, *Int. J. Numer. Methods Eng.* **24**, 763 (1987).

<sup>20</sup>W. H. A. Schilders, *Numerical Methods for Semiconductor Device Simulation* (Springer, Vienna, in press), Vols. I and II.

<sup>21</sup>M. Pope and C. E. Swenberg, *Electronic Processes in Organic Crystals and Polymers*, 2nd ed. (Oxford University Press, Oxford, 1999).

<sup>22</sup>P. Langevin, *Ann. Chim. Phys.* **28**, 433 (1903).

<sup>23</sup>A. Pivrikas, G. Juška, A. J. Mozer, M. Scharber, K. Arlauskas, N. S. Sariciftci, H. Stubb, and R. Österbacka, *Phys. Rev. Lett.* **94**, 176806 (2005).

<sup>24</sup>E. A. Schiff, *J. Non-Cryst. Solids* **190**, 1 (1995) and references therein.

<sup>25</sup>J. Shao and G. T. Wright, *Solid-State Electron.* **3**, 291 (1969).

<sup>26</sup>M. A. Lampert and P. Mark, *Current Injection in Solids*, 1st ed. (Academic, London, 1970).

<sup>27</sup>H. Bässler, *Phys. Status Solidi B* **175**, 15 (1993).

<sup>28</sup>C. Tanase, E. J. Meijer, P. W. M. Blom, and D. M. de Leeuw, *Phys. Rev. Lett.* **91**, 216601 (2003).

<sup>29</sup>H. C. F. Martens, H. B. Brom, and P. W. M. Blom, *Phys. Rev. B* **60**, R8489 (1999).

<sup>30</sup>S. Berleb and W. Brütting, *Phys. Rev. Lett.* **89**, 286601 (2002).

<sup>31</sup>P. Blood and J. W. Orton, *The Electrical Characterization of Semiconductors: Majority Carriers and Electron States* (Academic, San Diego, 1992).

<sup>32</sup>J. Nelson, *Phys. Rev. B* **67**, 155209 (2003).

<sup>33</sup>C. Melzer, E. J. Koop, V. D. Mihalechi, and P. W. M. Blom, *Adv. Funct. Mater.* **14**, 865 (2004).